

# Oil & Natural Gas Technology

DOE Award No.: DE-FE0009904

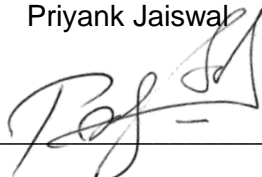
## Quarterly Research Performance Progress Report (Period ending 6/30/2015)

### Structural and Stratigraphic Controls on Methane Hydrate occurrence and distribution: Gulf of Mexico, Walker Ridge 313 and Green Canyon 955

Project Period: 10/01/2012 – 09/30/2015

Submitted by:

Priyank Jaiswal



Signature



Office of Fossil Energy

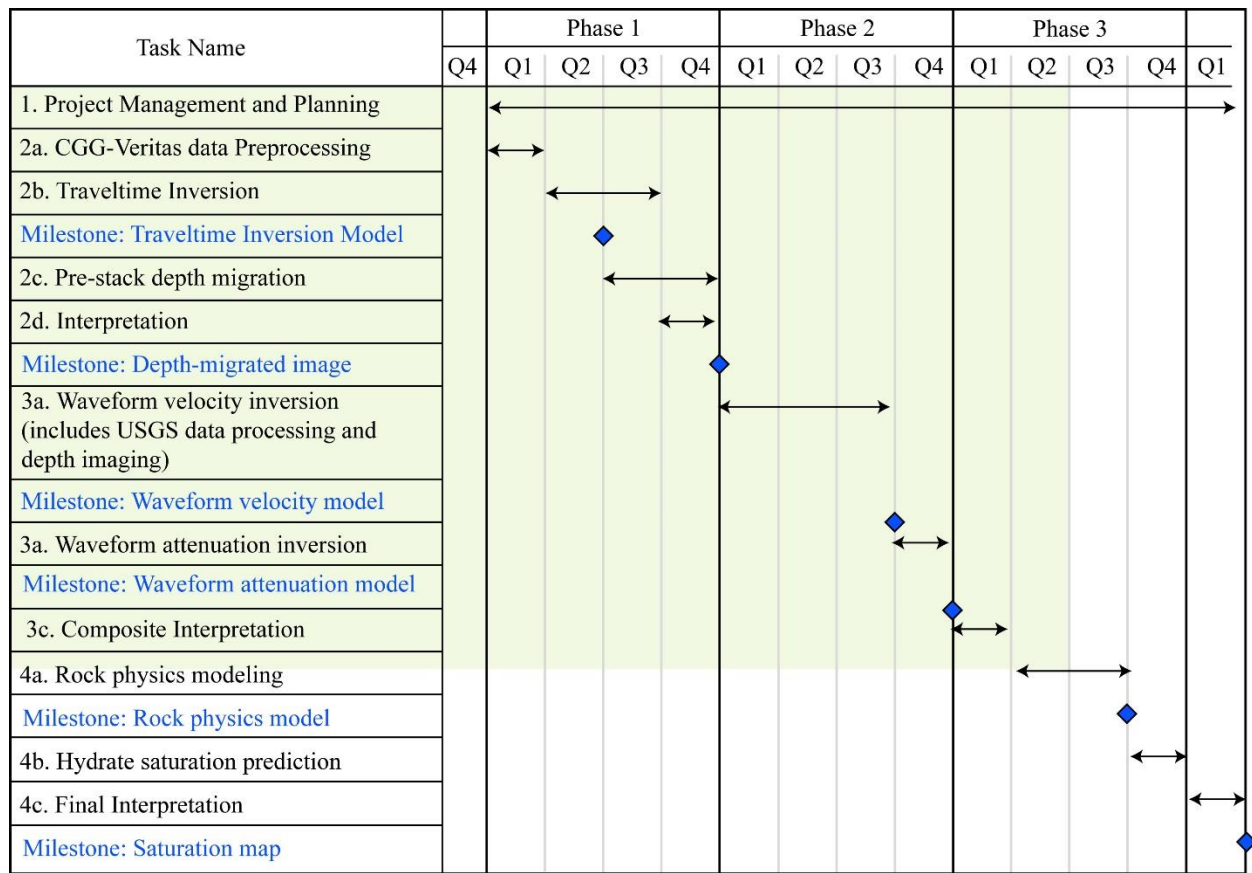


Table 1. Gantt chart. The project is on target till date. Tasks already completed in the milestone chart are shaded in green.

## Executive Summary

This quarterly progress summarizes the progress made towards completion of Phase 3, Subtask 4.1, “hydrate quantification at the log scale.” which comprises rock physics modeling of the P-wave log.

## Background

The overall objective is to identify and understand structural and stratigraphic controls on hydrate accumulation and distribution in leased blocks WR313 (WR: Walker Ridge) and GC955 (GC: Green Canyon) in the Gulf of Mexico using seismic and well data (Figure 1). The effort is to be completed in three phases. In the first phase, the objective is to create a large-sale (resolution in the order of Fresnel zone) P-wave velocity model using traveltime inversion and a corresponding depth image using pre-stack depth migration (PSDM). This phase was completed in due time. In the second phase, the objective was to jointly interpret the pre-stack depth migrated images and the full-waveform  $V_p$  models that were obtained as Phase 1 and Phase 2 deliverables. This phase was also completed in due time and a manuscript summarizing the efforts up till Phase 2 for GC955 was communicated to Journal of Geophysical Research – Solid Earth.

The third phase has two objectives. The first objective is to create a hydrate distribution map with the help of P-wave velocity and attenuation model created in the second phase and standard rock physics modeling method. This report describes rock physics modeling of the GC955-H well. The second objective is to jointly interpret all available datasets to determine the structural and stratigraphic controls on hydrate occurrence and distribution in GC955 and WR313.

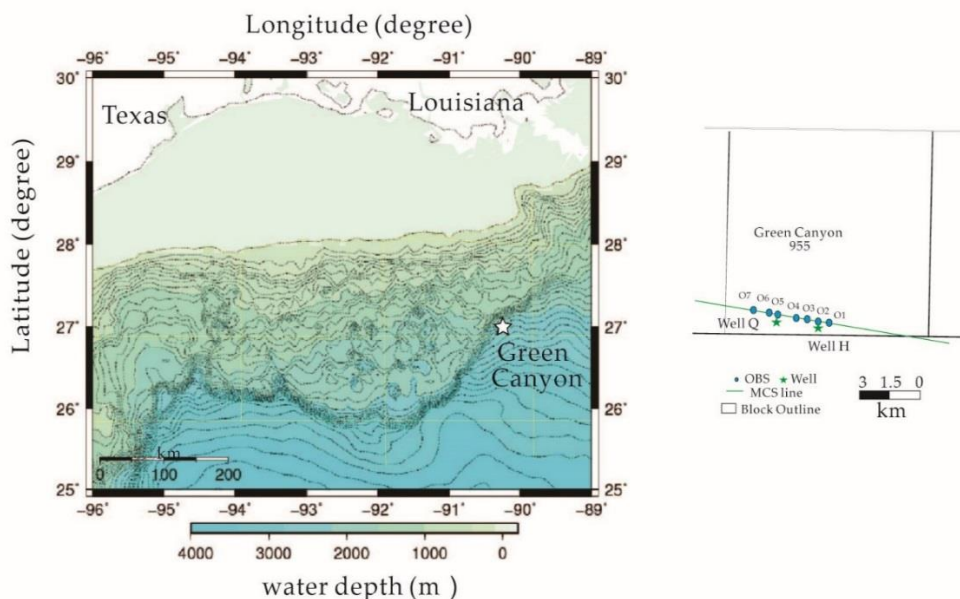


Figure 1: Base map. Seafloor bathymetry of Gulf of Mexico showing the location of the study area at the mouth of Green Canyon. The acquisition layout within lease block Green Canyon 955 (GC955) is shown in the inset. Solid line is the track of the multi-channel seismic (MCS) profile. Solid circles are location of ocean bottom seismometers (OBS) O1 – O7. Solid stars mark the locations of the wells Q and H that were drilling during the Joint Industry Project Leg II (JIP II).

## Approach

### Nomenclature

$R$ : Average radius of the grain

$\rho_s$ : Bulk density of solid phase.

$\rho_f$ : Bulk density of fluid (brine).

$\rho_h$ : Bulk density of hydrate.

$\bar{\rho}_f$ : New bulk density of the pore fluid mixture.

$\rho_b$ : Total bulk density of saturated sediments.

$\phi_t$ : Original total porosity

$\bar{\phi}$ : New total porosity (after hydrate is added to the mineral frame).

$\phi_c$ : Critical porosity

$S_h$ : Hydrate saturation of the pore space

$C_h$ : Volumetric concentration of hydrate in a unit volume of rock

$K_s$ : Bulk modulus of solid phase

$K_h$ : Bulk modulus of hydrate

$K_f$ : Bulk modulus of fluid (brine)

$\bar{K}_f$ : New bulk modulus of the pore fluid mixture.

$K_{HM}$ : Effective bulk modulus

$K_{dry}$ : Bulk modulus of dry frame

$K_{sat}$ : Bulk modulus of saturated sediments

$G_s$ : Shear modulus of solid phase

$G_{HM}$ : Effective shear modulus

$G_{dry}$ : Shear modulus of dry frame

$G_{sat}$ : Shear modulus of saturated sediments

$S_N$ : Normal stiffness between two grains in contact

$S_T$ : Tangential stiffness between two grains in contact

$\nu_s$ : Poisons ratio of solid phase

$\nu_{HM}$ : Effective poisons ratio

$P$ : Hydrostatic confining stress

$V_p$ : Compressional (P)-wave velocity and  $V_s$ : Shear (S)-wave velocity

$M$ : Compressional modulus

### Background

Pure gas hydrates have a P-wave velocity of about 3.27 km/s [Waite *et al.*, 2000]. The velocity of marine sediments within 300 m of water depth is generally accepted as 1.5 – 1.7 km/s. Presence of gas hydrates therefore alters the bulk P-wave velocity. Governed by thermodynamics and chemistry, hydrate exhibits a variety of growth styles in their host sediments [Clennell *et al.*, 1999; Tohidi *et al.*, 2001]. In coarse-grained sediments they occur as pore suspension, e.g. in the Nankai Prism [Kida *et al.*, 2009], grain displacing, e.g. in the Mackenzie Delta [Winters *et al.*, 2004], and contact cement, e.g., in the Oseberg Field [Dvorkin and Nur, 1996]. In fine-grained sediments, they also occur within fractures, e.g. in the Krishna-Godavari Basin [Collett *et al.*, 2008] and in massive forms, e.g. Gulf of Mexico [MacDonald *et al.*, 1994]. Presence of hydrate alters elastic velocities of their host sediments. The magnitude of the velocity change, however, does not just depend on the amount of the hydrate but also on their growth styles [Dai *et al.*, 2008a; Dai *et al.*, 2008b; Petersen *et al.*, 2007; Waite *et al.*, 2000]. In a forward sense, both the amount and growth style can be realized in the form of a rock physics model that can then be used for calculating elastic velocities through first-principle based methods [Mavko *et al.*, 2009]. The inverse, however, i.e., deducing the amount and growth-style of hydrate from a given elastic velocity model, is not straightforward.

In coarse-grained sediments, hydrates can exist in at least three states. It could be a) cement coat binding the grains (can also be modeled as hydrate being part of the mineral frame), b) non-cementing part of mineral frame which reduces porosity and effect on the solid phase elastic properties, and c) constituent of the pore fluid. These arrangements are illustrated in Figure 2.

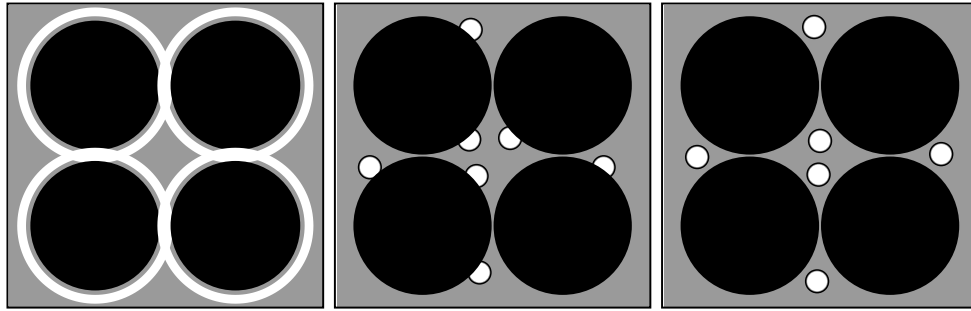


Figure 2: Three possible arrangement of methane hydrate in pore space (after [Dvorkin *et al.*, 2003]). The mineral grains are black; brine is gray; and hydrate is white.

In cases a) and b) hydrate is attached to the grains and therefore considered as mineral frame. The total porosity changes with the saturation,  $S_h$ , as:

$$\bar{\phi} = \phi_t - C_h = \phi_t (1 - S_h).$$

In case c) hydrate is not connected to grains and therefore considered as part of the pore fluid mainly affecting on the pore fluid elastic properties. The total porosity of the solid frame does not change with respect to  $S_h$  and therefore remains the same.

$$\bar{\phi} = \phi_t$$

However, the bulk modulus ( $\overline{K_f}$ ) of pore fluid changes as the harmonic average of hydrate ( $K_h$ ) and fluid ( $K_f$ ):

$$\overline{K_f} = [S_h / K_h + (1 - S_h) / K_f]^{-1},$$

Since the matrix remains unaffected, the shear modulus of the sediment remains unchanged but the bulk density ( $\overline{\rho_f}$ ) changes as the arithmetic average of hydrate ( $\rho_h$ ) and fluid ( $\rho_f$ ):

$$\overline{\rho_f} = S_h \rho_h + (1 - S_h) \rho_f.$$

This implies that morphology of grain to grain contact through hydrate cementing impacts the elastic moduli differently than grain to grain contact with hydrate in suspension. Thus, the same rock type with same porosity and identical mineralogy may be much stiffer in cemented case than those with no cement (Dvorkin *et al.*, 2003).

Helgerud et al. (1999) developed a method for modeling different hydrate arrangements in marine sediments known as “Effective Medium Modeling (EMM);” it is the method of choice in this applications. EMM is performed in two steps. First, elastic moduli of the dry sediment frame are estimated and second, the fluid is placed in the frame to compute the bulk elastic moduli of the system. The two steps are explained below:

#### 1) Building dry frame:

First, Bulk (K) and shear (G) modulus and density of solid phase are calculated using Hill’s (1952) average and mass balance equations:

$$K_s = 0.5 \cdot [\sum_{i=1}^m f_i K_i + (\sum_{i=1}^m f_i / K_i)^{-1}],$$

$$G_s = 0.5 \cdot [\sum_{i=1}^m f_i G_i + (\sum_{i=1}^m f_i / G_i)^{-1}],$$

$$\rho_s = \sum_{i=1}^m f_i \rho_i,$$

Where  $m$  is the number of the mineral components.  $f_i$  is fraction of  $i^{th}$  component in the mineral frame.  $K_i, G_i$  &  $\rho_i$  are the bulk, shear modulus and density of  $i^{th}$  component respectively.

Then, effective bulk ( $K_{HM}$ ) and shear ( $G_{HM}$ ) modulus are calculated to account for the effective pressure, porosity and mineralogy of the sediment. For this purpose,  $S_N$  and  $S_T$ ; the normal and tangential stiffnesses between two grains in contact respectively, are calculated.

$$S_N = \frac{4aG_s}{1 - \nu_s}, \quad S_T = f \frac{8aG_s}{2 - \nu_s}.$$

Where  $a$  is the radius of the circular contact area between the spheres and  $G_s$  and  $\nu_s$  are the shear modulus and Poisson's ratio of the material of the grains, respectively.  $f$  is a frictionless coefficient used to indicate grain contact type. It varies between 0 and 1. For instance, for 100% cement contact case (frictionless contact)  $f=0$ . As cement contacts decreases,  $f$  increases to maximum value of 1 indicating hydrates are in pore-filling mode (perfect adhesion).

$$K_{HM} = \frac{n(1-\phi_c)}{12\pi R} S_N, \quad G_{HM} = \frac{n(1-\phi_c)}{20\pi R} (S_N + \frac{3}{2} S_T),$$

Substitution  $S_N$  and  $S_T$  in effective moduli equation results the following:

$$K_{HM} = \left[ \frac{n^2(1-\phi_c)^2 G_s^2}{18\pi^2(1-\nu_s)^2} P \right]^{\frac{1}{3}},$$

$$G_{HM} = \frac{2+3f-\nu_s(1+3f)}{5(2-\nu_s)} \left[ \frac{3n^2(1-\phi_c)^2 G_s^2}{2\pi^2(1-\nu_s)^2} P \right]^{\frac{1}{3}},$$

$$\nu_{HM} = \frac{2-2f+\nu_s(2f-1)}{2[4+f-\nu_s(2+f)]}.$$

Where  $\phi_c$  is critical porosity (limit of the porosity at which the mineral grains can be viewed as being in suspension) which is estimated to be 0.35 to 0.4 for clastics (Nur *et al.*, 1998),  $n$  is the coordination number (the average number of contacts per grain) which is estimated by Dvorkin and Nur (1996) to be about 6 at critical porosity,  $R$  is the average radius of the grain, and  $S_N$  and  $S_T$  are the normal and tangential stiffnesses between two grains in contact respectively.  $P$  is hydrostatic confining stress.

In case of grains that are in perfect contact (frictionless spheres):

$$S_N = \frac{4aG_s}{1-\nu_s}, \quad S_T = 0$$

$$K_{HM} = \left[ \frac{n^2(1-\phi_c)^2 G_s^2}{18\pi^2(1-\nu_s)^2} P \right]^{\frac{1}{3}}, \quad G_{HM} = \frac{1}{5} \left[ \frac{3n^2(1-\phi_c)^2 G_s^2}{2\pi^2(1-\nu_s)^2} P \right]^{\frac{1}{3}}$$

$$\nu_{HM} = \frac{1}{2} \frac{(V_p/V_s)^2 - 2}{(V_p/V_s)^2 - 1} = \frac{1}{2} \left( 1 - \frac{3}{3K_{HM}/G_{HM} + 1} \right) = 0.25.$$

The effective Poisson's ratio is constant and does not depend on the material of grains.

In case of grains that are in least contact (perfect adhesion; [Mindlin, 1949]):

$$S_N = \frac{4aG_s}{1-\nu_s}, \quad S_T = \frac{8aG_s}{2-\nu_s},$$

$$K_{HM} = \left[ \frac{n^2(1-\phi_c)^2 G_s^2}{18\pi^2(1-\nu_s)^2} P \right]^{\frac{1}{3}}, \quad G_{HM} = \frac{5-4\nu_s}{5(2-\nu_s)} \left[ \frac{3n^2(1-\phi_c)^2 G_s^2}{2\pi^2(1-\nu_s)^2} P \right]^{\frac{1}{3}}.$$

$$\nu_{HM} = \frac{\nu_s}{2(5-3\nu_s)}$$

In case a combined situation comprising cemented and uncemented contacts between grains, original equations are used with a fractionless coefficient  $f$ :

$$S_N = \frac{4aG_s}{1-\nu_s}, \quad S_T = f \frac{8aG_s}{2-\nu_s}.$$

For porosity reduction effects on elastic moduli the two porosity states - critical porosity and porosity after hydrates inclusion – are connected using a rock model of choice for hydrates (pore filling, etc.). Three basic rock models can be envisioned [Dvorkin and Nur, 1996]:

- a) Stiff rock model: It is suited when hydrates are modeled as cement. This model adds hydrates as additional material within original grains affecting on grain to grain contact. This increases the elastic moduli and velocity rapidly even with small reduction in porosity as shown in Figure 15. This model implement the upper Hashin-Shtrikman bound.

$$K_{Dry} = \left[ \frac{\phi/\phi_c}{K_{HM} + \frac{4}{3}G_s} + \frac{1-\phi/\phi_c}{K_s + \frac{4}{3}G_s} \right]^{-1} - \frac{4}{3}G_s,$$

$$G_{Dry} = \left[ \frac{\phi/\phi_c}{G_{HM} + Z} + \frac{1-\phi/\phi_c}{G_s + Z} \right]^{-1} - Z,$$

$$Z = \frac{G_s}{6} \left( \frac{9K_s + 8G_s}{K_s + 2G_s} \right).$$

- b) Soft rock model: This model is suited for un-cemented hydrates in pore-filling mode. This model assumes small particles of hydrates fill pore spaces reducing the total porosity. In this case increment in velocity is relatively modest (Figure 4). This model applies the lower Hashin-Shtrikman bound to indicate elastic moduli versus porosity reduction.

$$K_{Dry} = \left[ \frac{\phi/\phi_c}{K_{HM} + \frac{4}{3}G_{HM}} + \frac{1-\phi/\phi_c}{K_s + \frac{4}{3}G_{HM}} \right]^{-1} - \frac{4}{3}G_{HM},$$

$$G_{Dry} = \left[ \frac{\phi/\phi_c}{G_{HM} + Z} + \frac{1-\phi/\phi_c}{G_s + Z} \right]^{-1} - Z,$$

$$Z = \frac{G_{HM}}{6} \left( \frac{9K_{HM} + 8G_{HM}}{K_{HM} + 2G_{HM}} \right).$$

- c) Constant cement model: This model is suited for a hybrid case. This model is used for partially cemented grains with hydrate in pore-filling mode. This model uses lower Hashin –Shtrikman bound but the high porosity end-point lies on the cement model curve (figure4).



$$K_{Dry} = \left[ \frac{\phi/\phi_c}{K_{HM} + \frac{4}{3}G_{HM}} + \frac{1-\phi/\phi_c}{K_s + \frac{4}{3}G_{HM}} \right]^{-1} - \frac{4}{3}G_{HM},$$

$$G_{Dry} = \left[ \frac{\phi/\phi_c}{G_{HM} + Z} + \frac{1-\phi/\phi_c}{G_s + Z} \right]^{-1} - Z,$$

$$Z = \frac{G_{HM}}{6} \left( \frac{9K_{HM} + 8G_{HM}}{K_{HM} + 2G_{HM}} \right).$$

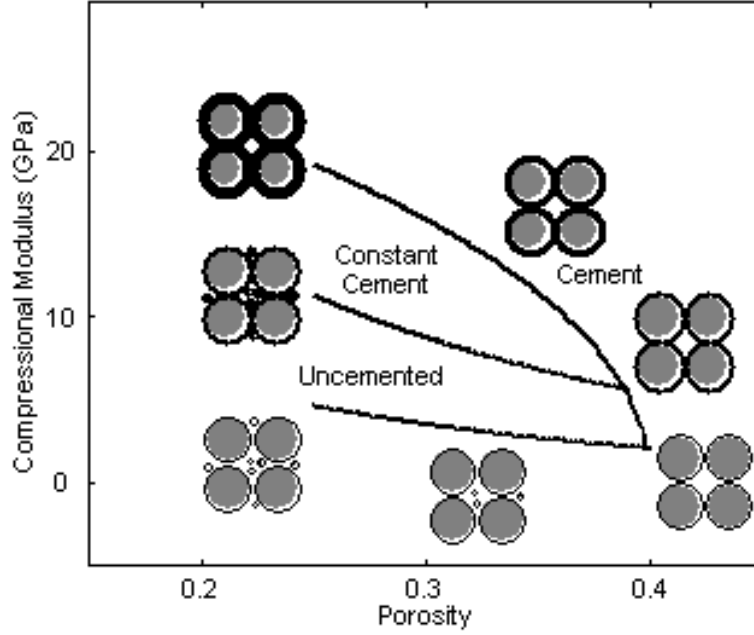


Figure 3: Compressional modulus versus porosity for three modes of porosity reduction (bold curves) for a dry pure-quartz porous system (after Dvorkin *et al.*, 2003).

## 2) Fluid emplacement

This step mainly comprises placing fluid in the dry frame to account for saturated sediments using [Gassmann, 1951] equation for Bulk (K) and Shear (G) moduli and Mavko *et al.* (1998) equation for compressional (M) modulus:

$$K_{Sat} = K_s \frac{\phi K_{Dry} - (1 + \phi) K_f K_{Dry} / K_s + K_f}{(1 - \phi) K_f + \phi K_s - K_f K_{Dry} / K_s}, \quad G_{Sat} = G_{Dry},$$

$$M_{Sat} = M_s \frac{\phi M_{Dry} - (1 + \phi) K_f M_{Dry} / M_s + K_f}{(1 - \phi) K_f + \phi M_s - K_f M_{Dry} / M_s},$$

Finally, the elastic-wave velocities,  $V_p$  and  $V_s$ , can be computed using the elastic moduli ( $K$ ,  $G$  and  $M$ ) and density ( $\rho$ ) as:

$$M = \rho V_p^2, \quad G = \rho V_s^2, \quad K = M - \frac{4}{3}G,$$

Where the bulk density can be defined as:  $\rho_b = (1 - \phi)\rho_s + \phi\rho_f$ .

### *Hydrates in fracture*

The faulted stratigraphy has been modeled by introducing dimensionless cracks within a sediment matrix. In our approach geometry of fractures is not required. Rather, fracture density is important. The modulus-porosity relation of the faulted stratigraphy is predicted using the Hashin Shtrikman bounds [Hashin and Shtrikman, 1963]; the lower bound assumes fractures are disconnected and therefore in the foreground and the upper bound assumes that fractures are interconnected and in the background.

The system is broken down into three phases; the first two phases are shale (clay and quartz) as matrix and water as pore-filling fluid. The third phase is faults which are completely filled with hydrates. Soft rock model is used to estimate the moduli of the two-phase component (shale filled with 100% water) and the third phase is tested with both upper and lower Hashin-Shtrikman bounds. The upper bound physically implies that the framework material is the stiffest material and the inclusions are filled with soft material. Since hydrates is the stiffest component, the Upper Hashin-Shtrikman bound can be applied to indicate fractures in connected mode.

The lower Hashin-Shtrikman bound indicates the original framework material in the system is the softest material, whereas the inclusions are filled with stiff material. Shale saturated with water is the softest component in the system, therefore, this bound can be used to best estimate hydrates mode in non-connected fractures (isolated fractures). See Jaiswal *et al.* [2014] for the model description.

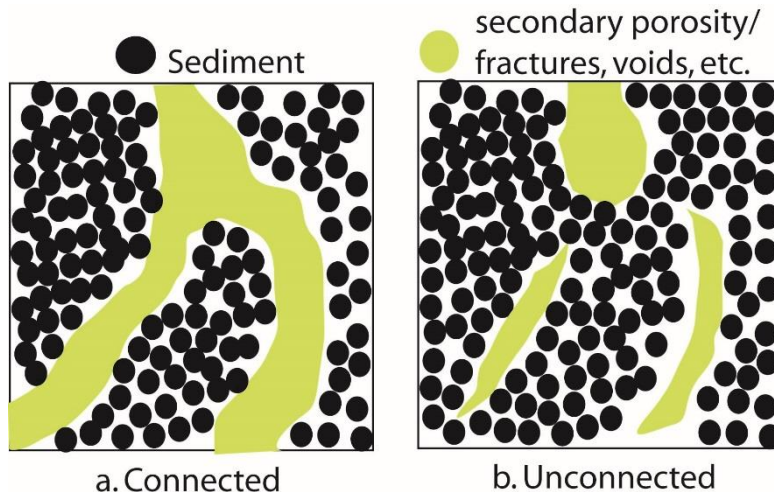


Figure 4: Hydrate in clay cartoon. (A) Hydrates in connected secondary-porosity/ fractures; and (D) Hydrate in unconnected secondary-porosity/ fractures.

It is expected that the state of the rock will be in between fully connected and fully unconnected fractures. The connectivity index allows the fractured system to vary between connected and unconnected states. It is calculated as follow:

$$CI = A + \beta \times Sat$$

where  $CI$ ,  $A$ ,  $\beta$  and  $Sat$  are Connectivity Index, constant, change rate and saturation respectively.

Well GC955-H was drilled through both hydrate-bearing clay and sand dominated stratigraphy. Using the models described above, hydrate saturations in this well is being presented for different scenarios.

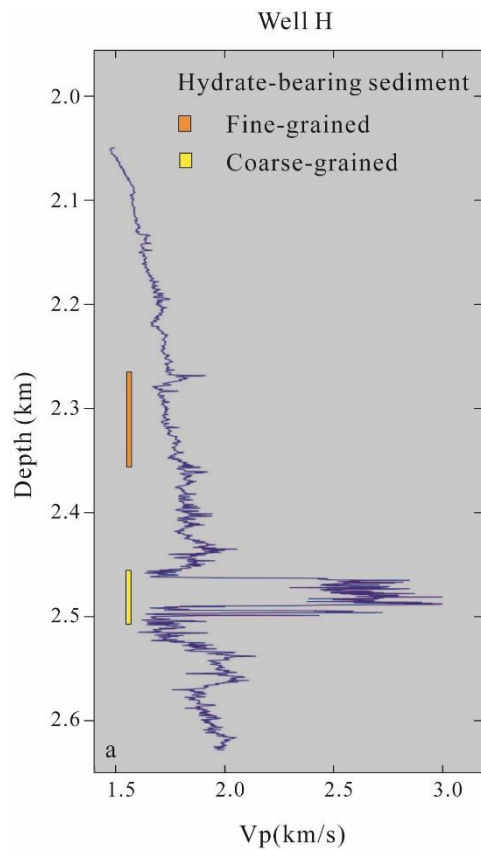


Figure 5. Well GC955 Vp log. Hydrate in the fine- and coarse grained stratigraphy has been confirmed through resistivity enhancements [Frye, 2010]. The log shows a reasonably significant increase in  $V_P$  at the level of sand-bearing unit but not in the clay-bearing unit.

## Results:

### *Hydrate in Sand*

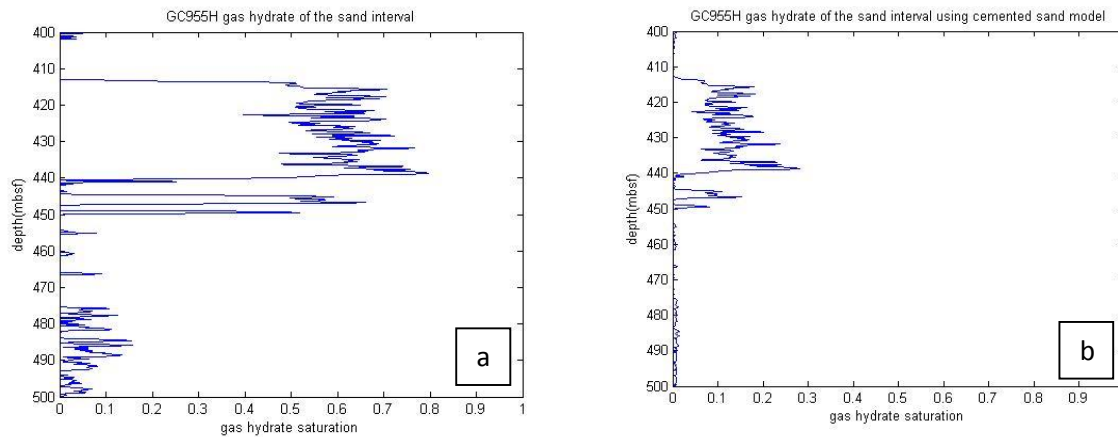


Figure 6. Hydrate saturation in sand computed assuming (a) hydrate in pore spaces and (b) hydrate as grain coating cement

For computing Figure 6 it is assumed that the entire sand interval is internally well connected.

### *Hydrate in Clay*

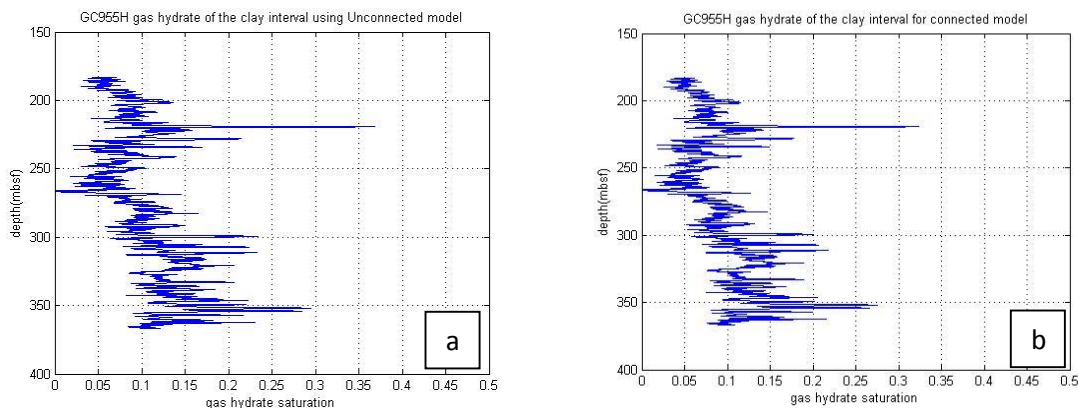


Figure 7. Hydrate saturation in clay assuming (a) unconnected fractures and (b) fully connected fractures.

For computing Figure 7 it is assumed that hydrate are only present in fractures and not within the sediment matrix.

## Conclusions:

Rock physics models of GC955-H Vp log suggest a different hydrate saturation under different modes of hydrate growth. In the sand layer, the saturation can be as high as 50% if hydrate growth is assumed in pore spaces only. If the growth is assumed as cement, the saturation is likely to be in the 15% range. In the clay layer, the saturation is overall low. Regardless of the connectivity assumption, the hydrate saturation in clay will be in 15% range. More accurate saturation prediction could not be done due to missing Shear-wave log.

**Milestone Status:**

Milestone	Description	Status	Schedule
Traveltime Inversion Model	The recipient shall compare the real and predicted reflection traveltimes from the final velocity model to be used for PSDM.	Done for CGGVeritas Dabase and for the USGS dataset	Completed on target
Depth Migrated Image	The recipient shall compare structure and stratigraphy between the final depth image and images in literature and SSRs.	Done	Completed on target
Waveform velocity model	The recipient shall compare waveform inversion velocity and sonic logs at well locations.	Done	Completed On target
Waveform attenuation model	The recipient shall compare real and synthetic simulated data.	Done	Completed On target
Rock physics model	The recipient shall compare predicted hydrate saturation at well locations with that available in the literature and methods of other DOE funded PIs, if available.	Ongoing	On target
Saturation map	The recipient shall compare consistency between hydrate distribution and structural/stratigraphic features interpreted in the study area.	Ongoing	On target

## References:

- Clennell, M. B., M. Hovland, J. S. Booth, P. Henry, and W. J. Winters (1999), Formation of natural gas hydrates in marine sediments 1. Conceptual model of gas hydrate growth conditioned by host sediment properties, *Journal of Geophysical Research-Solid Earth*, 104(B10), 22985-23003.
- Collett, T., M. Riedel, J. Cochran, R. Boswell, J. Presley, P. Kumar, A. Sathe, A. Sethi, M. V. Lall, and V. Sibal (2008), Expedition 01 Initial Reports Rep., New Delhi, India.
- Dai, J., F. Snyder, D. Gillespie, A. Koesoemadinata, and N. Dutta (2008a), Exploration for gas hydrates in the deepwater, northern Gulf of Mexico: Part I. A seismic approach based on geologic model, inversion, and rock physics principles, *Marine and Petroleum Geology*, 25(9), 830-844.
- Dai, J. C., N. Banik, D. Gillespie, and N. Dutta (2008b), Exploration for gas hydrates in the deepwater, northern Gulf of Mexico: Part II. Model validation by drilling, *Marine and Petroleum Geology*, 25(9), 845-859.
- Dvorkin, J., and A. Nur (1996), Elasticity of high-porosity sandstones: Theory for two North Sea data sets, *Geophysics*, 61(5), 1363-1370.
- Dvorkin, J., A. Nur, R. Uden, and T. Taner (2003), Rock physics of a gas hydrate reservoir, *The Leading Edge*, 22(9), 842-847.
- Frye, M. (2010), Gulf of Mexico Gas Hydrate Joint Industry Project: Overview of Leg II LWD Results.
- Gassmann, F. (1951), Elastic Waves Through A Packing Of Spheres, *Geophysics*, 16(4), 673-685.
- Hashin, Z., and S. Shtrikman (1963), A variational approach to the theory of the elastic behaviour of multiphase materials, *Journal of the Mechanics and Physics of Solids*, 11(2), 127-140.
- Jaiswal, P., S. Al-Bulushi, and P. Dewangan (2014), Logging-while-drilling and wireline velocities: Site NGHP-01-10, Krishna-Godavari Basin, India, *Marine and Petroleum Geology*.
- Kida, M., K. Suzuki, T. Kawamura, H. Oyama, J. Nagao, T. Ebinuma, H. Narita, H. Suzuki, H. Sakagami, and N. Takahashi (2009), Characteristics of Natural Gas Hydrates Occurring in Pore-Spaces of Marine Sediments Collected from the Eastern Nankai Trough, off Japan, *Energy & Fuels*, 23(11), 5580-5586.
- MacDonald, I. R., N. L. Guinasso, R. Sassen, J. M. Brooks, L. Lee, and K. T. Scott (1994), Gas hydrate that breaches the sea floor on the continental slope of the Gulf of Mexico, *Geology*, 22(8), 699-702.
- Mavko, G., T. Mukerji, and J. Dvorkin (2009), *The Rock Physics Handbook*, Second ed., Cambridge University Press, Cambridge, England.
- Mindlin, R. D. (1949), COMPLIANCE OF ELASTIC BODIES IN CONTACT, *J. Appl. Mech.-Trans. ASME*, 16(3), 259-268.
- Petersen, C. J., C. Papenberg, and D. Klaeschen (2007), Local seismic quantification of gas hydrates and BSR characterization from multi-frequency OBS data at northern Hydrate Ridge, *Earth and Planetary Science Letters*, 255(3-4), 414-431.
- Tohidi, B., R. Anderson, M. B. Clennell, R. W. Burgass, and A. B. Biderkab (2001), Visual observation of gas-hydrate formation and dissociation in synthetic porous media by means of glass micromodels, *Geology*, 29(9), 867-870.
- Waite, W. F., M. B. Helgerud, A. Nur, J. C. Pinkston, L. A. Stern, S. H. Kirby, and W. B. Durham (2000), Laboratory measurements of compressional and shear wave speeds through methane hydrate, *Gas Hydrates: Challenges for the Future*, 912, 1003-1010.
- Winters, W. J., I. A. Pecher, W. F. Waite, and D. H. Mason (2004), Physical properties and rock physics models of sediment containing natural and laboratory-formed methane gas hydrate, *American Mineralogist*, 89(8-9), 1221-1227.

## **National Energy Technology Laboratory**

626 Cochrans Mill Road  
P.O. Box 10940  
Pittsburgh, PA 15236-0940

3610 Collins Ferry Road  
P.O. Box 880  
Morgantown, WV 26507-0880

13131 Dairy Ashford Road, Suite 225  
Sugar Land, TX 77478

1450 Queen Avenue SW  
Albany, OR 97321-2198

Arctic Energy Office  
420 L Street, Suite 305  
Anchorage, AK 99501



Visit the NETL website at:

[www.netl.doe.gov](http://www.netl.doe.gov)